FAST LARGE VOLUME SIMULATIONS OF THE 21 CM SIGNAL FROM THE REIONIZATION AND PRE-REIONIZATION EPOCHS

M. G. SANTOS[1]
L. FERRAMACHO[1], M. B. SILVA[1], A. AMBLARD[2], A. COORAY[2]
[1] *CENTRA, Departamento de Física, Instituto Superior Técnico, 1049-001 Lisboa, Portugal*
[2] *Center for Cosmology, Department of Physics and Astronomy, University of California, Irvine, CA 92697*

We present a new type of simulation of the 21cm signal from the Reionization and pre-Reionization epoch capable of quickly generating the signal up to very high redshifts with the large field of view of the next generation of radio telescopes. This simulation uses a semi-numerical prescription based on 3-d Monte-Carlo realizations of the dark matter density field, achieving a much higher dynamical range than previous time-consuming N-body codes with radiative transfer algorithms. The simulation extends to high redshifts ($z \sim 25$) thus including the effect of the Lyman alpha and collisional coupling as well as X-ray heating and corrections due to the gas bulk velocities. With the new algorithm we were able to achieve very large volumes (1000 Mpc)^3, thus fully probing the large scale structure of the 21cm signal. This fast simulation also allows to quickly test the effect of different astrophysical parameters on the 21cm signal.

1 Introduction

Observations of the 21 cm line of neutral hydrogen are currently considered to be one of the most promising probes of the epoch of reionization (EoR) and possibly even the preceding period, during the so called dark ages. Motivated by the observational possibilities offered by the current and upcoming low frequency radio interferometers[a,b,c] a great deal of effort has been underway in order to fully understand and generate the expected 21 cm signal that will be seen by these experiments (see Furlanetto et al.[4] for a review). Numerical simulations can potentially provide an improved description of the 21 cm brightness temperature signal but are slow to run, being constrained in dynamical range to sizes typically smaller than 100 Mpc/h. We propose a semi-numerical technique, capable of quickly generating an end-to-end simulation of the 21 cm signal even at high redshifts when the spin temperature is non-negligible. Moreover, this method can be used to simulate very large volumes (e.g. 1000 Mpc), crucial to simulate the field-of-view of next generation of radio telescopes, without sacrificing the speed or requiring unpracticable amounts of computer memory. The code to generate this type of simulation is now provided publicly online[d] and it will be subject to continuous improvement through calibration against full radiative transfer/hydrodynamic simulations. The large volume simulations created with

[a] LOFAR: http://lofar.org
[b] MWA: http://web.haystack.mit.edu/arrays/MWA
[c] SKA: http://www.skatelescope.org
[d] http://www.simfast21.org

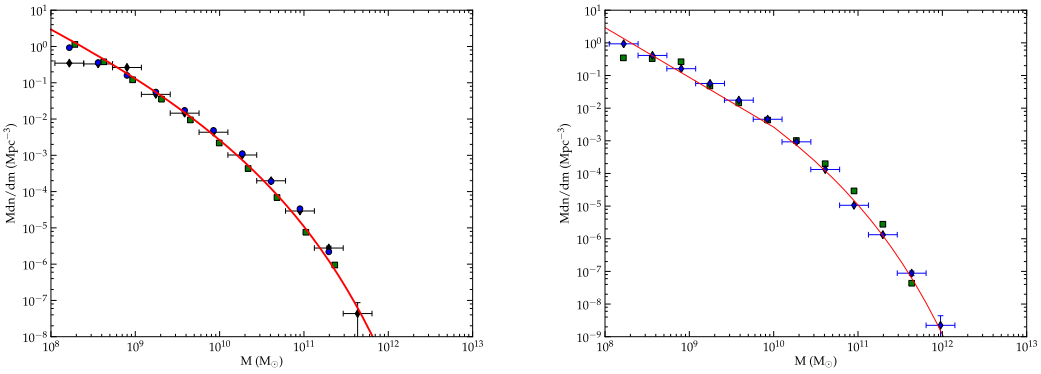

Figure 1: Left: Mass functions at z=10 taken from our halo filtering prescription with L=142 Mpc and N=1536^3 (blue circles) and L=300 Mpc and N=1800^3 (black diamonds). The results for the N-body simulation of Trac et al.[13] with L=142 Mpc are also shown as green squares. The red line shows the theoretical mass function. Right: mass function for our simulation with L=300Mpc and N=1800^3 (green squares) compared with the large volume simulation with L=1000 Mpc and N=1800^3 (blue diamonds).

this method are part of the SKA Design Studies Simulated Skies initiative and we hope this approach can prove useful to generate sky models for the future 21 cm experiments, which is crucial to test for calibration issues and foreground removal methods.

2 From linear density fluctuations to the ionization field

The underlying basis for our simulation is the Monte-Carlo generation of the dark matter linear density field assuming a Gaussian probability distribution function for the linear overdensity as the initial state, which is then later evolved and used to find the collapsed structures and the corresponding ionized bubbles. This implementation partially follows the algorithm prescribed in Mesinger & Furlanetto[7], which is based on the "peak-patch" approach introduced by Bond & Myers[1]. Figure 1 shows the obtained halo mass function. In the left panel, we can see that our simulations agree quite well with the theoretical curve and N-body simulation, although the number of low mass halos in the simulation with the lower resolution (L=300 Mpc) is slightly underestimated. However, we have checked that this effect has a minor impact on the ionized hydrogen distribution and can be seen as a good compromise in order to cover the largest possible volume with this algorithm.

The positions of both the halos and the dark matter were then corrected to include non-linear dynamics using the Zel'dovich approximation[16] and with the corrected halo and density fields, the ionization regions can be determined using a similar excursion-set algorithm. The principle behind this procedure is that the galaxies formed inside dark matter halos will produce a given amount of photons (dependent of the halo mass) that will ionize the surrounding hydrogen generating ionized bubbles. The efficiency of this process can be quantified by one parameter ζ. Figure 2 shows two slices of our ionization field at the beginning and ending of reionization. These figures exhibit the characteristic bubble structure of ionized hydrogen increasing in size at lower redshifts until converging into a completely ionized IGM. In order to characterize the statistical distribution of the ionization field we computed its power spectrum, $P_{x_i x_i}$ (figure 3). We see that the excursion-set formalism allows to obtain a bubble power spectrum that matches the one from a full N-body radiative transfer simulation when the volume size and cell resolution are the same. However, at large scales we find an increase in power with larger boxes, which we believe is due to the fact that we are finding larger bubbles in the 300 Mpc box, while smaller bubbles are absorbed in larger ones.

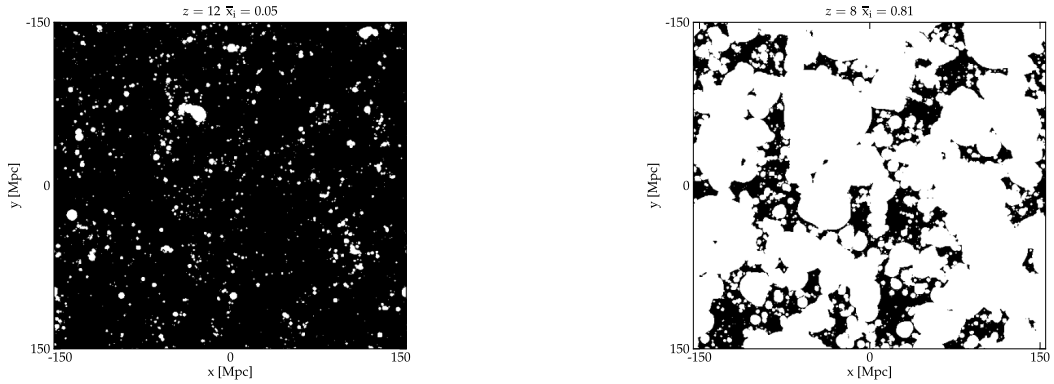

Figure 2: Slices of the ionization field at the beginning and ending of reionization (left: $z = 12$, $\bar{x}_i = 0.05$; right: $z = 8$, $\bar{x}_i = 0.81$)

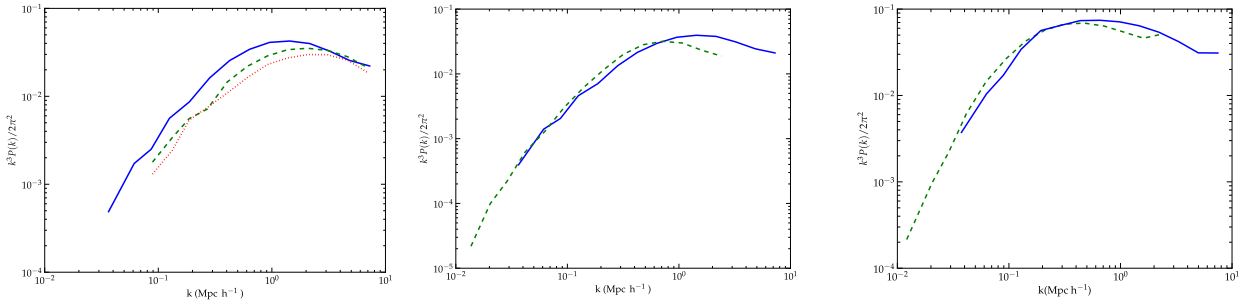

Figure 3: First panel: power spectrum of the ionization field for our simulation with L=143 Mpc,N=768^3 (red dotted curves), L=300 Mpc,N=600^3 (solid blue curves) and the simulation of Trac et al.[13] with L=143 Mpc,N=768^3 (dashed green curves), for $z = 9$ and $\bar{x}_i = 0.15$. The boxes were smoothed to a common resolution. Two right panels: power spectrum of the ionization field for the very large volume simulation (green dashed curves), compared to the same result for the L=300 Mpc simulation. Both plots are for z=9 but using different efficiency parameters (ζ=5.0 and ζ=14.0) so that $\bar{x}_i = 0.1$ (left) and $\bar{x}_i = 0.55$ (right).

3 Extending the simulation to very large volumes

Although quite fast, the semi-numerical simulation presented so far still imposes some limitations regarding the volume it can cover since it requires a very large number of cells in order to achieve sufficient resolution to filter scales corresponding to $10^8 M_\odot$ halos and cover large volumes at the same time. However, we can use a low resolution box and use the expected halo mass function to place the smaller halos in our large volume simulation cells by following the prescription of Wilman et al.[14]. By the definition of the mass function, the quantity $n = dn/dM\Delta M\Delta V$ corresponds to the mean number of halos that can be found in a given cell with comoving volume ΔV. If one would simply perform a Poisson sampling for each cell with a mean n, the distribution of obtained halos would yield a correct mass function but their positions would be completely random. In order to correlate the halo positions with the underlying density field, a normalized bias term can be added,

$$n_{cell} = Ke^{b(z,M)\delta(z)} \frac{dn}{dM} \Delta M \delta V \ , \tag{1}$$

where $b(z, M)$ is the bias model for halos at a given redshift and $\delta(z, M)$ the density field at the same redshift. The factor K is a normalization constant that ensures the consistency of the above expression with the mass function $\frac{dn}{dM}$ when averaging over the large volume box. The above equation introduces a dependence of the halo locations on the density field, by amplifying

the overdense regions with respect to underdense ones. As for the bias term, it describes the difference in clustering between dark matter halos and the mass density field.

We have then used this prescription in complement with the excursion-set formalism to perform a dark matter simulation with L=1000 Mpc. In figure 1 right panel, we plot (blue diamonds) the obtained mass function for this run and compare it to the higher resolution, L=300 Mpc simulation obtained using only the excursion set formalism. We also checked that this formalism can reproduce the spatial distribution of halos with its correlation with the underlying matter density field. We then proceed to derive the ionization bubbles using the same method as in Section 2. The results for the power spectrum of the ionization field are shown in figure 3 (two right panels) compared to those obtained with the full excursion-set method with L=300 Mpc and for two different efficiency parameters at z=9. The curves seem to agree reasonable well showing convergence with the 300 Mpc box, although if we go to even larger ionization fractions we still find slightly larger bubbles in the 1Gpc box (the largest bubble for the 1Gpc box with $x_i = 0.55$ has a size of 20 Mpc).

4 The 21 cm signal up to z=25

With ionization maps at different redshifts we can focus on the predicted 21 cm signal from neutral hydrogen during the pre-EOR and the EOR. At high redshifts ($z > 10$) the spin temperature (T_S) is no longer high enough to saturate the effect in the brightness temperature and we need to take into account the contribution of fluctuations from the spin temperature to the 21 cm signal. These originate from fluctuations in the coupling between the spin temperature and the gas temperature and the perturbations in the gas temperature itself (T_K) and we can write:

$$1 - \frac{T_\gamma}{T_S} = \frac{x_{tot}}{1 + x_{tot}} \left(1 - \frac{T_\gamma}{T_K}\right), \tag{2}$$

where $x_{tot} = x_\alpha + x_c$ is the sum of the radiative and collisional coupling parameters. Collisions can be important for decoupling the HI 21 cm spin temperature from the CMB, especially at very high redshifts ($z > 30$) [8] and are straightforward to apply to the simulation [6]. The radiative coupling due to the absorption of Ly_α photons (the Wouthysen-Field effect[15,3]), on the other hand, should be dominant for $z < 25$ and we shall concentrate on calculating this effect here. The radiative coupling is given by

$$x_\alpha = \frac{S_\alpha J_\alpha}{J_c}, \tag{3}$$

with $J_c \approx 5.552 \times 10^{-8}(1+z)$ m^{-2}s^{-1}Hz^{-1}sr^{-1} and S_α is a correction factor of order unity[5,2,4]. We follow the prescription in Santos et al.[9] to calculate J_α. For this, we need the comoving star formation rate, $\psi(\mathbf{x}, z)$ and $\epsilon_\alpha(\nu)$, the spectral distribution function of the sources (defined as the number of Ly_n photons per unit frequency emitted at ν per baryon in stars). We can easily assume any model for $\epsilon_\alpha(\nu)$ in our code to test for different sources of radiation. For this simulation we used: $A\nu^{-\alpha}$, with $\alpha = 0.9$ and A set such that we get a total of 20000 Lyα photons per baryon. We used the halo catalogue to obtain the star formation rate density which was then normalized to the one in Shin et al.[12]. The gas in the IGM is also heated as the reionization progresses. In our simulation, we assume that this heating is done by x-rays with an emission connected to the star formation rate (see Santos et al.[9]). This X-ray emissivity is again assumed to be a power law, with a spectral index and amplitude compatible with what is observed for starburst galaxies. Figure 4 left panel, shows the evolution of the gas temperature with redshift, where we can see that most of the IGM is heated above 100K for $z < 11$. The spin temperature starts very close to the CMB one (no signal) and approaches the gas temperature as x_α increases, following it for $z < 17$.

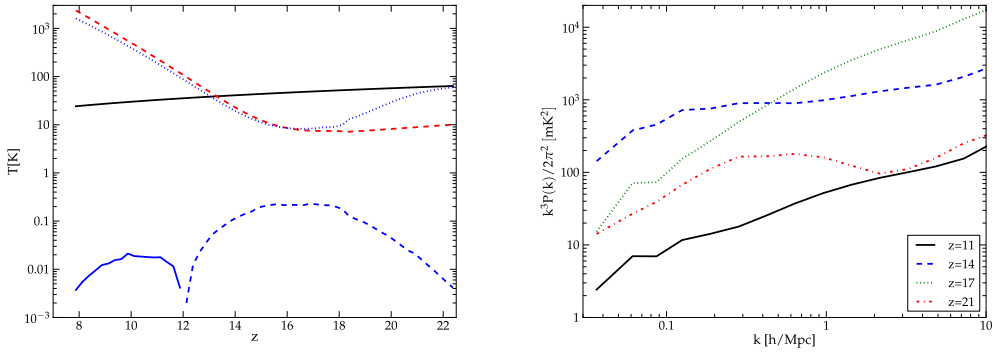

Figure 4: Left: the evolution of the gas temperature, spin temperature and brightness temperature with redshift. Solid black line - CMB; Red dashed - gas temperature; Blue dotted - spin temperature; Dark blue solid/dashed (below) - brightness temperature. Right: The power spectrum of the 21-cm signal at high redshifts including all fluctuations in the spin temperature.

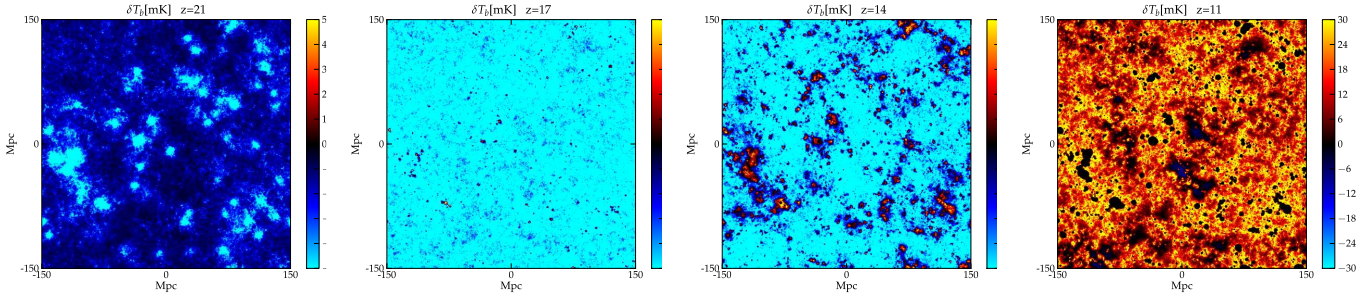

Figure 5: Maps of the 21 cm signal at very high redshifts from the simulation, including all sources responsible for the fluctuations.

Putting it all together we can calculate the 21 cm signal. Calculation of x_α and the gas temperature takes around 5 minutes for each redshift in our machine using 20 CPUs. In figure 4 left panel, we can also see the evolution of the average brightness temperature with redshift, which is observed in absorption down to $z = 12$ where it becomes approximately zero when $T_K \approx T_{CMB}$. In figure 5 we show maps of the 21 cm signal for a few very high redshifts taking into account all the effects while figure 4 right panel, shows the corresponding power spectrum. At high redshifts ($z = 21$) most of the temperature is zero ($T_s \sim T_{CMB}$) but we already start to see some cold spots where the Lyα sources couple the spin temperature to the cold gas temperature and the fluctuations in x_α dominate. At $z = 17$ the spin temperature is basically following the gas one everywhere and we can see fluctuations in the 21 cm signal due essentially to the gas temperature (although most of the Universe is still cold at this epoch). At $z = 14$ we can already see the higher temperature regions surrounding the light sources located in the halos. Finally at $z = 11$ basically all the IGM is heated above the CMB and we start seeing the ionization bubbles ($\bar{x}_i \approx 0.1$, but note that some of the dark regions here are not due to the ionized bubbles but because $T_S = T_K \sim T_{CMB}$).

5 Summary

We presented a semi-numerical method capable of quickly generating end-to-end simulations of the 21 cm signal even at the high redshifts where the spin temperature is non-negligible (see Santos et al.[10] for further details). The algorithm allows to generate brightness temperature boxes with very large volumes, e.g. $(1000\ \mathrm{Mpc})^3$, crucial to properly simulate the field of view

of the next generation of radio-telescopes. The corresponding code (SimFast21) takes about 1 hour to run for each redshift, which can be considered remarkably fast. We are expecting that further optimization of the code can still reduce this time. This is on going research that will be implemented as we update the numerical code. Although much faster than hydrodynamical numerical simulations, our analysis shows that relevant quantities such as the halo mass function, the halo mass power spectrum or the ionization fraction power spectrum are all consistent with the numerical simulations with which we compared our results to. The dependence on the astrophysical parameters of the simulation was encoded in three functions: the ionization efficiency, ζ, the Ly_α spectral distribution function of the sources, ϵ_α and the X-ray spectral distribution function, ϵ_X. These functions can be easily changed for a model of our choice and the code can then quickly generate new simulations of the signal (even faster if we keep the same cosmology). By combining all the unknowns into a physically meaningful small set of parameters we can easily probe the huge intrinsic parameter space available to 21 cm observations. The code is now publicly available and we welcome the community participation in its updating and upgrading as well as development of additional applications on observational probes of reionization beyond the 21 cm observations.

Acknowledgements

This work was partially supported by FCT-Portugal under grant PTDC/FIS/66825/2006. This work was supported by the European Commission Framework Program 6, Project SKADS, Square Kilometre Array Design Studies (SKADS), contract no 011938.

References

1. Bond, J. R. & Myers, S. T. 1996, ApJS, 103, 1
2. Chuzhoy, L. & Shapiro, P. R. 2007, ApJ, 655, 843
3. Field, G. B. 1959, ApJ, 129, 536
4. Furlanetto, S. R., Oh, S. P., & Briggs, F. H. 2006, Phys. Rep., 433, 181
5. Hirata, C. M. 2006, MNRAS, 367, 259
6. Kuhlen, M., Madau, P., & Montgomery, R. 2006, ApJ, 637, L1
7. Mesinger, A. & Furlanetto, S. 2007, ApJ, 669, 663
8. Nusser, A. 2005, MNRAS, 359, 183
9. Santos, M. G., Amblard, A., Pritchard, J., et al. 2008, ApJ, 689, 1
10. Santos, M. G., Ferramacho, L., Silva, M. B., Amblard, A., & Cooray, A. 2009, ArXiv e-prints, MNRAS2010
11. Sheth, R. K. & Tormen, G. 1999, MNRAS, 308, 119
12. Shin, M.-S., Trac, H., & Cen, R. 2007, ArXiv e-prints, 708
13. Trac, H., Cen, R., & Loeb, A. 2008, ApJ, 689, L81
14. Wilman, R. J., Miller, L., Jarvis, M. J., et al. 2008, MNRAS, 388,1335
15. Wouthuysen, S. A. 1952, AJ, 57, 31
16. Zel'Dovich, Y. B. 1970, A&A, 5, 84